Human Molecular Genetics, 2010, Vol. 19, No. 21 **4145–4159**
doi:10.1093/hmg/ddq334
Advance Access published on August 12, 2010

Flt-1 haploinsufficiency ameliorates muscular dystrophy phenotype by developmentally increased vasculature in *mdx* mice

Mayank Verma[1,2,3], Yoko Asakura[1,2,3], Hiroyuki Hirai[1,2,3], Shuichi Watanabe[1,2,3], Christopher Tastad[1,2,3], Guo-Hua Fong[5], Masatsugu Ema[6], Jarrod A. Call[2,4], Dawn A. Lowe[2,4] and Atsushi Asakura[1,2,3,*]

[1]Stem Cell Institute, [2]Paul and Sheila Wellstone Muscular Dystrophy Center, [3]Department of Neurology and [4]Department of Physical Medicine and Rehabilitation, University of Minnesota Medical School, Minneapolis, MN, USA, [5]Center for Vascular Biology, University of Connecticut Health Center, University of Connecticut School of Medicine, Farmington, CT, USA and [6]Department of Anatomy and Embryology, Institute of Basic Medical Sciences, University of Tsukuba, Tsukuba, Japan

Received March 19, 2010; Revised and Accepted August 5, 2010

Duchenne muscular dystrophy (DMD) is an X-linked recessive genetic disease caused by mutations in the gene coding for the protein dystrophin. Recent work demonstrates that dystrophin is also found in the vasculature and its absence results in vascular deficiency and abnormal blood flow. This induces a state of ischemia further aggravating the muscular dystrophy pathogenesis. For an effective form of therapy of DMD, both the muscle and the vasculature need to be addressed. To reveal the developmental relationship between muscular dystrophy and vasculature, *mdx* mice, an animal model for DMD, were crossed with *Flt-1* gene knockout mice to create a model with increased vasculature. Flt-1 is a decoy receptor for vascular endothelial growth factor, and therefore both homozygous (*Flt-1*$^{-/-}$) and heterozygous (*Flt-1*$^{+/-}$) *Flt-1* gene knockout mice display increased endothelial cell proliferation and vascular density during embryogenesis. Here, we show that *Flt-1*$^{+/-}$ and *mdx:Flt-1*$^{+/-}$ adult mice also display a developmentally increased vascular density in skeletal muscle compared with the wild-type and *mdx* mice, respectively. The *mdx:Flt-1*$^{+/-}$ mice show improved muscle histology compared with the *mdx* mice with decreased fibrosis, calcification and membrane permeability. Functionally, the *mdx:Flt-1*$^{+/-}$ mice have an increase in muscle blood flow and force production, compared with the *mdx* mice. Consequently, the *mdx:utrophin*$^{-/-}$*:Flt-1*$^{+/-}$ mice display improved muscle histology and significantly higher survival rates compared with the *mdx:utrophin*$^{-/-}$ mice, which show more severe muscle phenotypes than the *mdx* mice. These data suggest that increasing the vasculature in DMD may ameliorate the histological and functional phenotypes associated with this disease.

INTRODUCTION

Duchenne muscular dystrophy (DMD) is an X-linked muscle disease affecting one in 3000 children where the gene that codes for the protein dystrophin is mutated (1). Dystrophin is a membrane-stabilizing protein that is part of the dystrophin-associated protein complex which protects the membrane integrity in response to contraction-induced damage (2). In dystrophic muscle where this linkage is disrupted, muscle fibers develop normally but are easily damaged. Damaged muscle fibers degenerate, and new fibers, recruited from satellite cells, regenerate in their place. However, regeneration is inefficient, so successive rounds of degeneration lead to a gradual replacement of muscle by connective tissue.

*To whom correspondence should be addressed at: Stem Cell Institute, McGuire Translational Research Facility, University of Minnesota, Room 4-220, 2001 6th Street. SE, Minneapolis, MN 55455, USA. Tel: +1 6126247108; Fax: +1 6126242436; Email: asakura@umn.edu

Abnormal blood flow is expected to induce muscle damage as first demonstrated by Mendell *et al*. (3). This group showed that ischemia through microvascular infarction produces a grouping of necrotic fibers, a phenotype routinely observed in DMD-afflicted muscle. Recent studies demonstrate that dystrophin is also detected in vascular smooth muscle of mice (4,5). The absence of dystrophin in the vasculatures of *mdx* mice (6), an animal model for DMD, results in the vascular abnormalities that may impair blood flow. This is through lower nitric oxide (NO)-dependent flow (shear stress)-induced endothelium-dependent dilation, endothelial NO synthase and neuronal NO synthase expression, as well as decreased vascular density (7,8). In addition, utrophin, a dystrophin homologue, expression in endothelium was also reported (9). Furthermore, disruption of the sarcoglycan complex, which is associated with dystrophin in vascular smooth muscle, perturbs vascular function. This initiates cardiomyopathy and exacerbates muscular dystrophy (10). Therefore, blood flow regulation might be disturbed in DMD, possibly increasing muscle damage. Recent work elegantly demonstrates the importance of dystrophin expression in vascular smooth muscle for muscle function of *mdx* mice. Ito *et al*. (5) generated smooth muscle-specific dystrophin transgenic *mdx* mice (*SMTg/mdx*) expressing dystrophin only in the smooth muscle driven by a smooth muscle-specific promoter. *SMTg/mdx* mice showed restoration of the NO-dependent modulation of α-adrenergic vasoconstriction and a partially improved muscle phenotype. Taken together, these reports suggest that impaired vascular function is associated with muscular pathology in DMD. Therefore, DMD is characterized by increased muscle damage and an abnormal blood flow after muscle contraction. This is termed the state of functional ischemia.

A two-hit hypothesis is proposed for pathogenic defects in the dystrophin–glycoprotein complex in muscular dystrophy (11): the first hit is a reduction in NO-mediated protection against ischemia in dystrophic muscle, and the second hit is an increase in cellular susceptibility to metabolic stress. Until now, the cause–effect relationship between the pathogenesis of DMD and functional ischemia has been unclear. Recent work demonstrates that the vasoactive drug tadalafil, a phosphodiesterase 5 inhibitor, administered to *mdx* mice ameliorated muscle damage, strongly indicating that functional ischemia is necessary to cause contraction-induced muscle fiber damage (12). However, the developmental relationship between muscular dystrophy and angiogenesis has yet to be discovered. Definitive treatment for muscular dystrophies will likely require that the dystrophin protein complex is restored in all affected muscle groups as well as vasculature to improve muscle function.

Vascular endothelial growth factor (VEGF) regulates angiogenesis through the promotion of endothelial cell growth, survival and migration. VEGF interacts with its receptors VEGFR-1 (Flt-1) and VEGFR-2 (Flk-1), which are expressed in hemangioblasts and endothelial cell lineages during developmental stage and tissue regeneration (13,14). Flt-1 is a typical tyrosine kinase receptor, and the tyrosine kinase domain of Flt-1 possesses much weaker activity than that of Flk-1. In addition to the full-length receptor, a soluble form of Flt-1 is produced via alternative splicing. Both the full-length and soluble form of Flt-1 possess strong binding affinity for VEGF (15). Mice lacking *Flt-1* gene display early embryonic lethality due to an overgrowth of endothelial cells and a disorganization of blood vessels (13–15). In contrast, heterozygous *Flt-1* gene knockout mice survive until adulthood and display relatively normal development. Kearney *et al*. (16) have shown that both heterozygous and homozygous *Flt-1* gene knockout mice display increased endothelial cell differentiation in embryonic stem cell cultures. These observations suggested that Flt-1 is a negative regulator for endothelial growth and differentiation during development. Several works demonstrate that administration of VEGF facilitates angiogenesis in muscle after ischemia (17). In addition, administration of VEGF can promote the growth of myogenic fibers, protect myogenic cells from apoptosis and eventually stimulate muscle regeneration (18). In *mdx* mice, administration of VEGF can improve both muscle histology and function (19). However, it remains unclear whether developmentally upregulated angiogenesis affects muscular dystrophy phenotype.

To address whether we could compensate for the state of functional ischemia found in the *mdx* mouse muscle by developmentally increasing the vascular density, we crossed *mdx* mice with the heterozygous *Flt-1* gene knockout mice ($Flt\text{-}1^{+/-}$) in which vascular density is increased. We then compared the dystrophic phenotypes between the *mdx*:$Flt\text{-}1^{+/-}$ and the control *mdx*:$Flt\text{-}1^{+/+}$ mice.

RESULTS

Heterozygous *Flt-1* gene knockout mice show an increase in vascular density

Mice lacking *Flt-1* gene by the insertion of β-galactosidase gene ($Flt\text{-}1^{-/-}$) display early embryonic lethality due to an overgrowth of endothelial cells and a disorganization of blood vessels (13–15). Current work showed that heterozygous *Flt-1* gene knockout ($Flt\text{-}1^{+/-}$) mice survive until adulthood and display no obvious phenotype. We compared vascular density between the wild-type ($Flt\text{-}1^{+/+}$) and heterozygous *Flt-1* knockout ($Flt\text{-}1^{+/-}$) new born and adult mice. Both $Flt\text{-}1^{+/-}$ new born and adult mice (505.5 ± 24.5 and 273.7 ± 14.4, respectively) clearly showed increased vascular density in the tibialis anterior (TA) muscle compared with their wild-type litter mates ($Flt\text{-}1^{+/+}$) (373.5 ± 23.5 and 172.6 ± 13.3, respectively) as expressed by the endothelial cell marker CD31 in cross-section (Fig. 1A and B). Fluorescence-activated cell sorting (FACS) analysis also confirmed the increased $CD31^+$ endothelial cells in the TA muscle of $Flt\text{-}1^{+/-}$ mice compared with the wild-type $Flt\text{-}1^{+/+}$ mice (Fig. 2A and B). These results suggest that $Flt\text{-}1^{+/-}$ mice display increased angiogenesis during postnatal muscle development. This observation is consistent with the published work that vasculogenesis is increased in $Flt\text{-}1^{+/-}$ embryonic stem cell cultures and that Flt-1 negatively regulates angiogenesis during development (16).

mdx mice are an animal homologue for DMD and display continuous degeneration and regeneration with subsequent calcium deposits and fibrosis in their muscle (20,21). It is important to determine whether angiogenesis affects DMD muscle pathology and function. For this purpose, we created

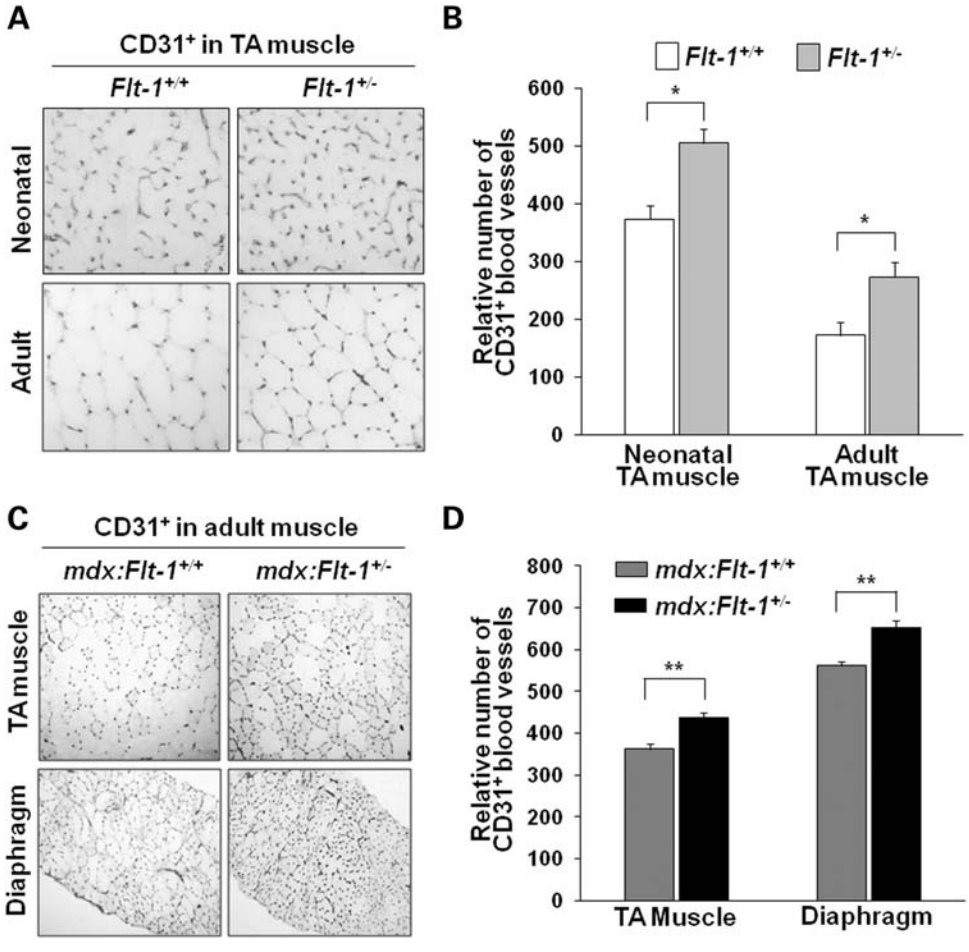

Figure 1. Increase in blood vessel density in the *Flt-1*$^{+/-}$ mouse background. Blood vessel density was measured by anti-CD31 antibody staining on cryosections. (**A**) Representative images of CD31-stained cryosections from the neonatal and adult TA muscle of the wild-type (*Flt-1*$^{+/+}$) and *Flt-1*$^{+/-}$ mice. (**B**) Relative number of CD31-positive blood vessels per view field in cross-sections of the TA muscle of neonatal ($n = 4$ each) and adult wild-type (*Flt-1*$^{+/+}$) and *Flt-1*$^{+/-}$ mice ($n = 6$ each). (**C**) Representative images of anti-CD31-stained cryosections of the control *mdx:Flt-1*$^{+/+}$ and *mdx:Flt-1*$^{+/-}$ mice. (**D**) Relative number of CD31-positive blood vessels per view-field in cross-sections of TA and diaphragm muscle of the *mdx:Flt-1*$^{+/+}$ and *mdx:Flt-1*$^{+/-}$ mice ($n = 12$ each). Values are mean ± SEM. Asterisks or double asterisks indicate experimental pairs where differences between the compared values were statistically significant ($P < 0.05$ or $P < 0.01$, respectively).

double-mutant *mdx* mice with the heterozygous allele for *Flt-1* (*mdx:Flt-1*$^{+/-}$) and compared them with their litter mates of *mdx* mice with the wild-type *Flt-1* alleles (*mdx:Flt-1*$^{+/+}$). The control *mdx:Flt-1*$^{+/+}$ mice had an average of 362 ± 12 and 562 ± 12 capillaries per view-field for the TA muscle and diaphragm, respectively. The *mdx:Flt-1*$^{+/-}$ mice had higher averages of 438 ± 10 and 653 ± 17 for the TA muscle and diaphragm, respectively (Fig. 1C and D). Similar increases in CD31^{+} endothelial cells in the *mdx:Flt-1*$^{+/-}$ mice compared with the control *mdx:Flt-1*$^{+/+}$ mice were also confirmed by FACS analysis of the TA muscle (Fig. 2A and B). The relatively frequent occurrence of dystrophin-positive revertant muscle fibers has been observed in *mdx* mice. The *mdx-5cv* mice used for this study have ~10-fold fewer revertants than the original *mdx* mice (22). Western blot analysis and immunostaining were performed on TA muscle extracts and sections to confirm that the expression of dystrophin and dystrophin-positive revertant fibers were not altered between *mdx:Flt-1*$^{+/+}$ and *mdx:Flt1*$^{+/-}$ mice (Fig. 3A–D).

It is known that, in the absence of dystrophin, the expression of utrophin, a dystrophin homologue, is enhanced to compensate for the membrane instability in *mdx* mice (23). The expression of utrophin was evaluated by western blot of the TA muscle extract. As expected, the expression of utrophin was upregulated in *mdx:Flt-1*$^{+/+}$ and *mdx:Flt1*$^{+/-}$ mice compared with the wild-type and *Flt1*$^{+/-}$ mice but was not altered between the wild-type and *Flt1*$^{+/-}$ mice or between the *mdx:Flt-1*$^{+/+}$ and *mdx:Flt1*$^{+/-}$ mice (Fig. 3C and E). Therefore, the *mdx:Flt-1*$^{+/-}$ mice and the control *mdx:Flt-1*$^{+/+}$ mice were utilized for further comparison to reveal the relationship between muscular dystrophy and angiogenesis in *mdx* mice.

Muscle morphology and histology were improved in *mdx:Flt-1*$^{+/-}$ mice

Evans blue dye (EBD) uptake is used as a measure of membrane permeability (24,25). The *mdx:Flt-1*$^{+/+}$ mice clearly showed some EBD-positive degenerating muscle fibers in

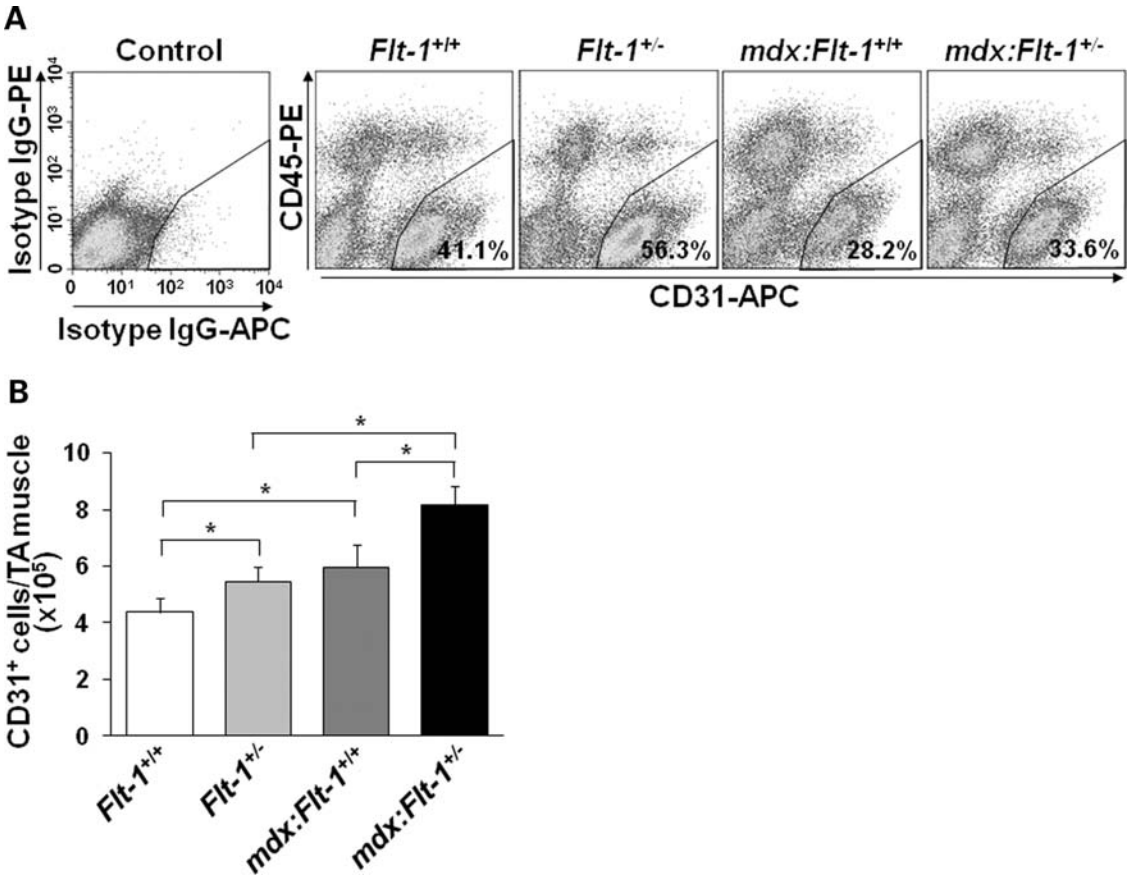

Figure 2. Increase in $CD31^+$ endothelial cells in the *Flt-1*$^{+/-}$ mouse background. (**A**) FACS analysis shows that the dissociated cells from the TA muscle of the *Flt-1*$^{+/-}$ and *mdx:Flt-1*$^{+/-}$ mice contained increased amount of $CD45\text{-}PE^-$ $CD31\text{-}APC^+$ endothelial cells in the gated areas compared with the wild-type (*Flt-1*$^{+/+}$) and *mdx:Flt-1*$^{+/+}$ mice, respectively. Control indicates the FACS profile for the control antibodies. (**B**) Total number of $CD45^-$ $CD31^+$ endothelial cells per TA muscle was estimated by data from the FACS analysis. Values are mean ± SEM ($n = 3$). Asterisks indicate experimental pairs where differences between the compared values were statistically significant ($P < 0.05$).

the TA muscle (3.30% ± 1.11) and in the diaphragm (3.02% ± 0.66) (Fig. 4A and B). On the other hand, the *mdx:Flt-1*$^{+/-}$ mice showed lower EBD-positive muscle fibers in the TA muscle (0.021% ± 0.05) and in the diaphragm (1.25% ± 0.25). These data strongly suggest that muscle fibers in the *mdx:Flt-1*$^{+/-}$ mice are more stable and less degenerative than the control *mdx:Flt-1*$^{+/+}$ mice.

Histological phenotypes commonly associated with DMD include excessive fibrosis and calcification. Fibrosis is the replacement of muscle fibers by fibrous connective tissue, which not only decreases the amount of force generators but also impedes the force generated by other muscle due to its inelastic properties (21,26). The diaphragm showed improvements for fibrosis in the *mdx:Flt-1*$^{+/-}$ mice (524.8 ± 43.4) compared with the control *mdx:Flt-1*$^{+/+}$ mice (372.4 ± 34.7) (Fig. 4C and D). In addition, the diaphragm in the control *mdx:Flt-1*$^{+/+}$ mice showed a large amount of calcium accumulation that can be seen macroscopically although being mostly absent in the *mdx:Flt-1*$^{+/-}$ mice (Fig. 4E and F). Alizarin red staining confirmed that the *mdx:Flt-1*$^{+/-}$ had far fewer calcium deposits, which were also generally smaller in size compared with the control *mdx:Flt-1*$^{+/+}$ mice. In contrast, as reported previously (21), fibrosis and calcification were not as prevalent in the TA muscle of the control *mdx:Flt-1*$^{+/+}$ mice (data not shown).

Centrally located nuclei (CLN) in muscle fibers are a typical phenotype associated with many different types of muscular dystrophies (21). The *mdx:Flt1*$^{+/-}$ mice displayed 50.00% ± 1.05 of fibers as having CLN compared with the control *mdx:Flt1*$^{+/+}$ mice, which showed 66.16% ± 2.06 of fibers with CLN (Fig. 5A and B). This value is similar to what has been found by others for the *mdx* mice (27). The drop in CLN in the *mdx:Flt1*$^{+/-}$ mice was also seen in the diaphragm compared with the control *mdx:Flt1*$^{+/+}$ mice (31.97 ± 0.77 versus 38.01 ± 0.50). Therefore, lower CLN in the *mdx:Flt1*$^{+/-}$ mice is indicative of the decreased fiber turnover and increased muscle fiber stability.

Muscle fiber type changes and hypertrophy development have been reported in *mdx* mouse muscle as compensation for the loss of force-generating capacity of the existing muscle. To determine the oxidative profile of the muscle, sections were stained for NADH-tetrazolium reductase (TR). The *mdx:Flt1*$^{+/-}$ mice (oxidative: 9.8 ± 2.6, oxidative-glycolytic: 56.9 ± 0.4, glycolytic: 33.2 ± 2.5) showed an increase in the amount of oxidative and oxidative-glycolytic fibers and a decrease in glycolytic fibers compared with the control

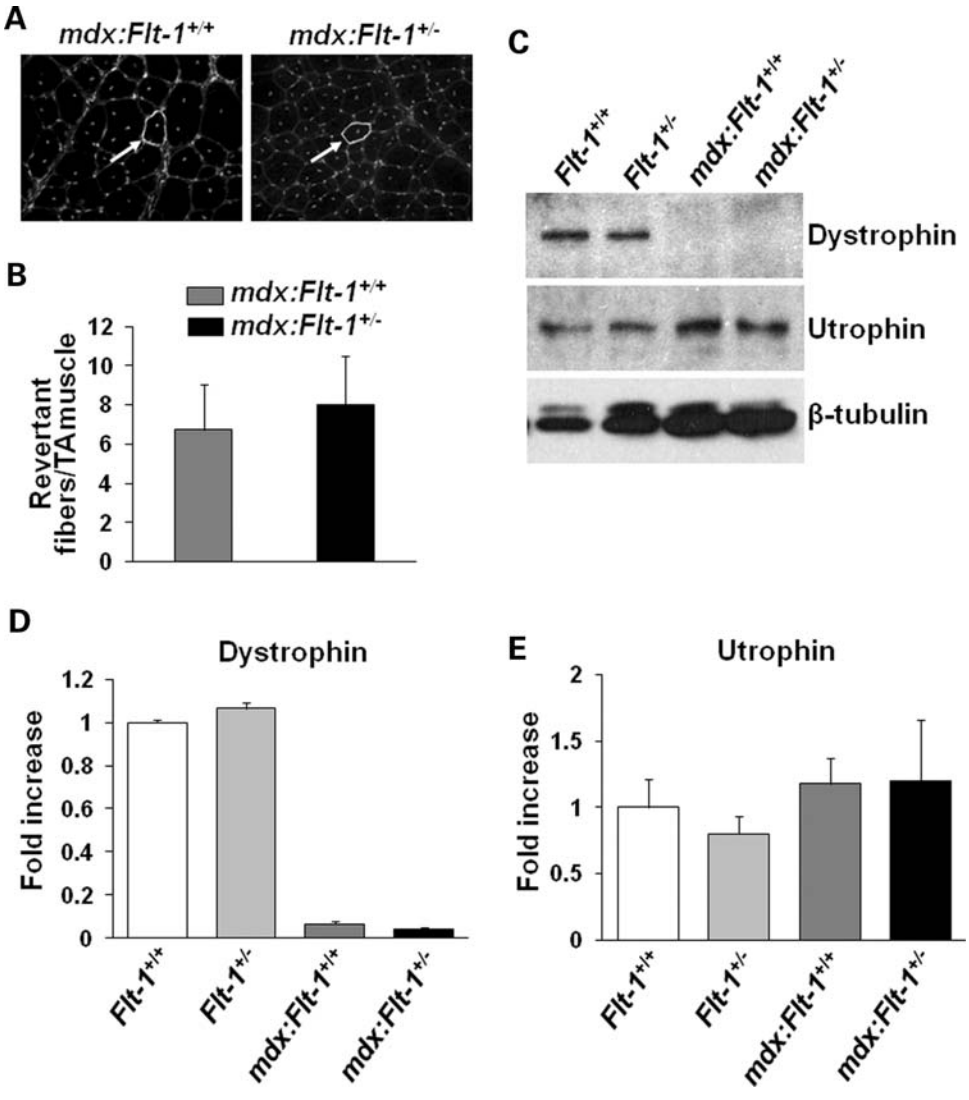

Figure 3. No change in dystrophin or utrophin expression in the TA muscle of the *mdx:Flt-1*$^{+/-}$ mice. (**A**) Representative images from TA muscle sections of the control *mdx:Flt-1*$^{+/+}$ and *mdx:Flt-1*$^{+/-}$ mice stained with anti-dystrophin antibody to detect revertant fibers. Arrows indicate dystrophin^{+} revertant fibers and DAPI staining indicates nuclei (blue). (**B**) Quantification of dystrophin-positive revertant fibers in the TA muscle of the control *mdx:Flt-1*$^{+/+}$ ($n = 4$) and *mdx:Flt-1*$^{+/-}$ ($n = 3$) mice. (**C**) Representative western blotting to detect dystrophin and utrophin proteins in the wild-type (*Flt-1*$^{+/+}$), *Flt-1*$^{+/-}$, *mdx:Flt-1*$^{+/+}$ and *mdx:Flt-1*$^{+/-}$ mice. β-tubulin was used for loading control. (**D**) Expression of dystrophin was unchanged in *Flt-1*$^{+/-}$ compared with the wild-type (*Flt-1*$^{+/+}$) mice ($n = 3$ each). Dystrophin is absent in the *mdx:Flt-1*$^{+/+}$ and *mdx:Flt-1*$^{+/-}$ mice ($n = 3$ each). (**E**) Expression of utrophin was unchanged by the *Flt-1*$^{+/-}$ background ($n = 3$ each). Values are mean ± SEM.

mdx:Flt1$^{+/+}$ mice (oxidative: 6.58 ± 0.5, oxidative-glycolytic: 50.5 ± 1.3, glycolytic: 42.8 ± 1.7) (Fig. 5C and D). Immunostaining using antibodies against the slow isoform of myosin heavy chain (MHC) (28,29) revealed an increase in the oxidative type I muscle fibers (*mdx:Flt1*$^{+/-}$: 1.74 ± 0.4, *mdx:Flt1*$^{+/+}$: 0.6 ± 0.2) (Supplementary Material, Fig. S1A and B). We also found that the mean fiber diameter size distribution in the *mdx:Flt1*$^{+/-}$ mice is skewed towards the smaller fiber size (Supplementary Material, Fig. S1C and D). This decrease in size may be due to a fiber type switch from glycolytic to oxidative type since oxidative fibers tend to be smaller than the glycolytic fibers. Alternatively, muscle in the *mdx:Flt1*$^{+/-}$ mice may contain reduced hypertrophic muscle compared with the control *mdx:Flt1*$^{+/-}$ mice.

mdx:Flt1$^{+/-}$ mice display increased blood perfusion

To evaluate whether the increase in vascular density also caused an increase in perfusion to the skeletal muscle, we measured the laser Doppler flow (LDF) in the TA muscle. The mean amount of flux is shown in perfusion units (PU) as per the manufacturer's recommendation (Fig. 6A). The *Flt-1*$^{+/-}$ (54.8 ± 1.2) and *mdx:Flt-1*$^{+/-}$ (62.6 ± 4.7) showed increased red blood cell (RBC) flux compared with the *wild-type Flt-1*$^{+/+}$ (46.1 ± 1.1) and *mdx:Flt-1*$^{+/+}$ (48.1 ± 3.3), respectively. This is consistent with the increase in blood vessel density seen in the TA muscle and may compensate for the functional ischemic phenotype observed in the *mdx* mice.

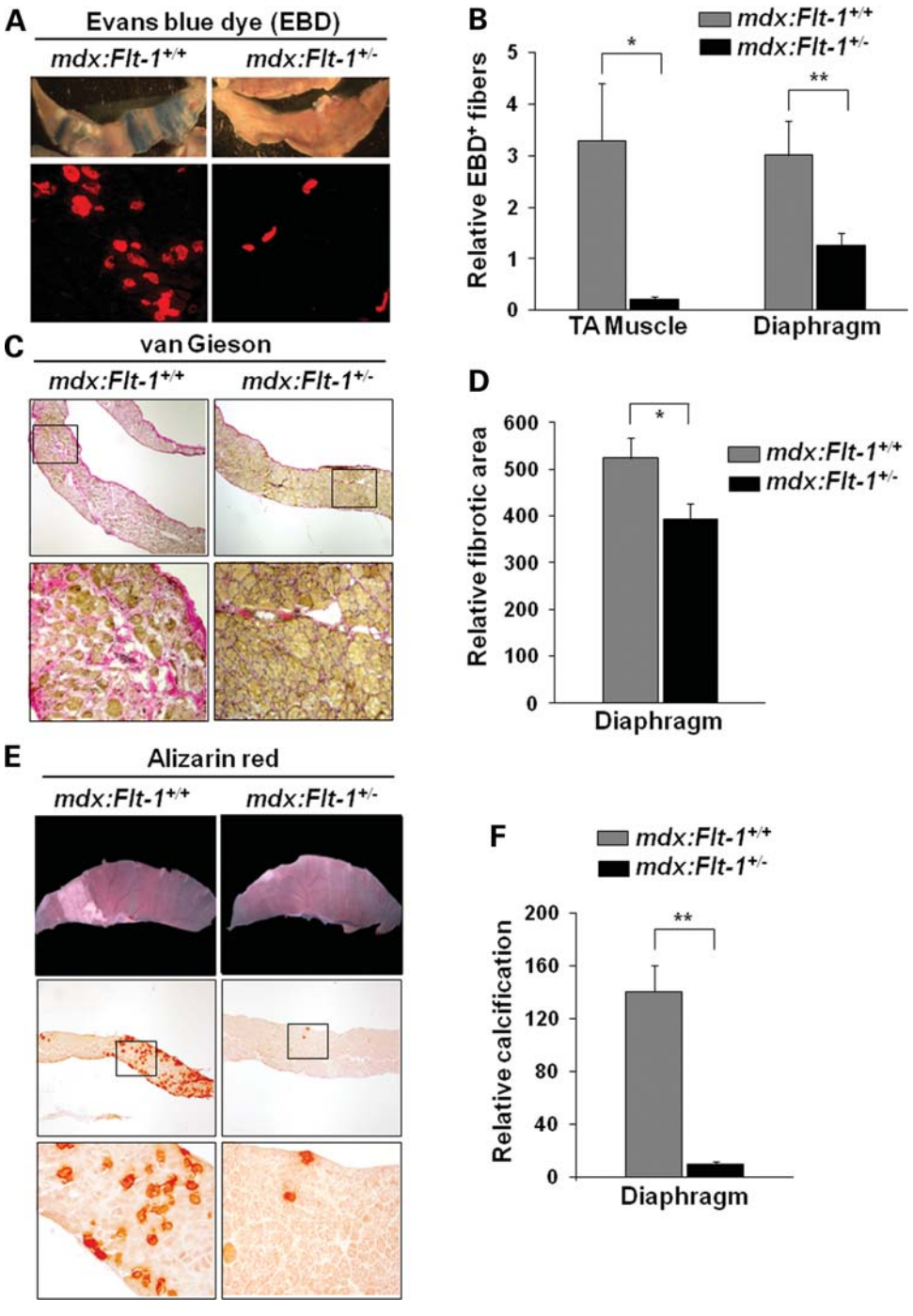

Figure 4. *mdx:Flt-1*$^{+/-}$ double-mutant mice display improved muscle pathology. (**A**) Representative images from whole diaphragm muscle of the control *mdx:Flt-1*$^{+/+}$ and *mdx:Flt-1*$^{+/-}$ mice injected with EBD. Blue staining denotes EBD uptake (upper panels). Cross-sections show EBD uptake in damaged TA muscle fibers of the *mdx:Flt-1*$^{+/+}$ and *mdx:Flt-1*$^{+/-}$ mice (lower panels: red fluorescence). (**B**) Quantification of EBD-positive fibers normalized by muscle area. *mdx:Flt-1*$^{+/-}$ double-mutant mice display decreased membrane damage in both the TA muscle and the diaphragm ($n = 9$ each) compared with the control *mdx:Flt-1*$^{+/+}$ ($n = 7$ each). (**C**) van Gieson staining on diaphragm cross-sections shows fibrosis (pink color) in the *mdx:Flt-1*$^{+/+}$ and *mdx:Flt-1*$^{+/-}$ mice (upper panels). Lower panels show magnified views from upper panels. (**D**) Quantification of relative fibrotic area in the diaphragm of *mdx:Flt-1*$^{+/+}$ and *mdx:Flt-1*$^{+/-}$ ($n = 5$ each) mice as evaluated by van Gieson stain. (**E**) Whole diaphragm shows calcium deposits on the muscle fibers of the *mdx:Flt-1*$^{+/+}$ and *mdx:Flt-1*$^{+/-}$ mice (white color: upper panels). Cryosections stained using Alizarin red for calcification (red color: middle panels). (**F**) Quantification of the relative calcified area of diaphragm of the *mdx:Flt-1*$^{+/+}$ and *mdx:Flt-1*$^{+/-}$ mice ($n = 6$ each) as evaluated by Alizarin red staining (lower panels). Values are mean ± SEM. Asterisks or double asterisks indicate experimental pairs where differences between the compared values were statistically significant ($P < 0.05$ or $P < 0.01$, respectively).

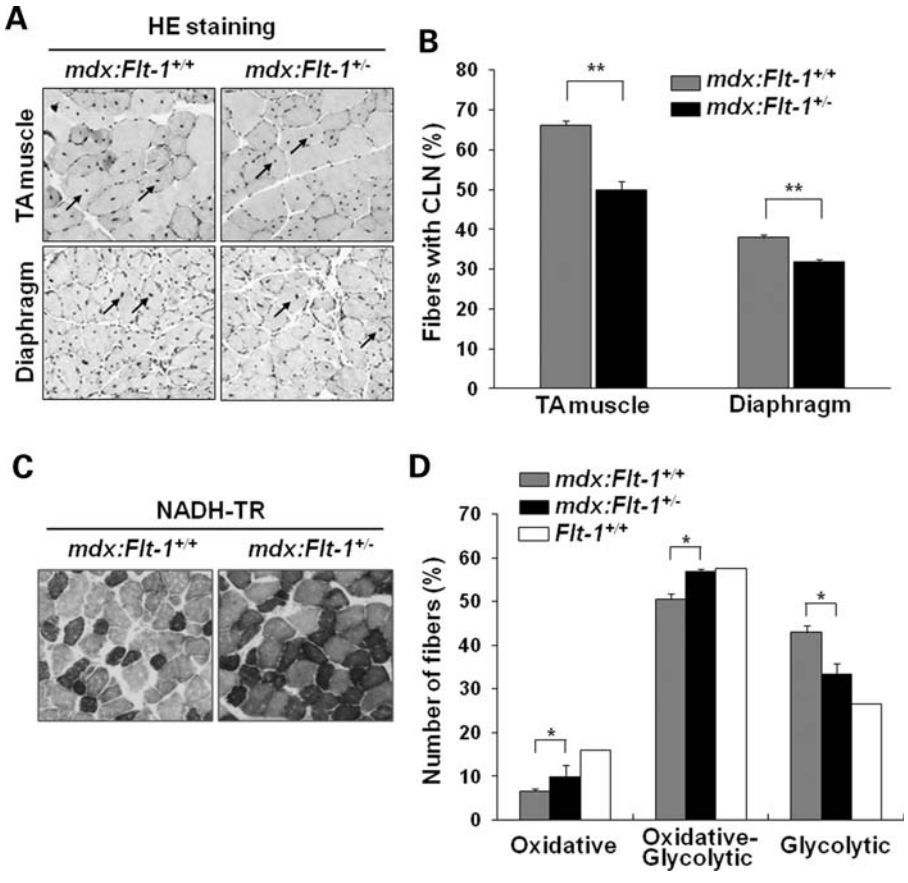

Figure 5. *mdx:Flt-1*$^{+/-}$ double-mutant mice display increased muscle fiber stability. (**A**) HE staining of the TA muscle and diaphragm cross-sections of the *mdx:Flt-1*$^{+/+}$ and *mdx:Flt-1*$^{+/-}$ mice. Arrows indicate muscle fibers with CLN. (**B**) Quantification of the percent of CLN in the TA muscle and diaphragm in the *mdx:Flt-1*$^{+/+}$ ($n = 4$ each) and *mdx:Flt-1*$^{+/-}$ mice ($n = 6$ and 4), respectively. (**C**) NADH-TR staining was used to distinguish oxidative (dark color), oxidative-glycolytic (intermediate color) and glycolytic (unstained or lightly stained) muscle fibers in the TA muscle of the *mdx:Flt-1*$^{+/+}$ and *mdx:Flt-1*$^{+/-}$ mice. (**D**) Fiber type distribution shows the *mdx:Flt-1*$^{+/-}$ mice ($n = 4$) had higher oxidative and oxidative-glycolytic fibers and fewer glycolytic fibers compared with the *mdx:Flt-1*$^{+/+}$ mice ($n = 4$). Wild-type (*Flt-1*$^{+/+}$) mice ($n = 4$) display the highest oxidative fiber distribution. Values are mean ± SEM. Asterisks or double asterisks indicate experimental pairs where differences between the compared values were statistically significant ($P < 0.05$ or $P < 0.01$, respectively).

mdx:Flt-1$^{+/-}$ mice display improved muscle contractile function

To examine whether the histological improvements translated into a functional improvement, local force production was measured in the hind limb. Maximum isometric torque was measured by quantifying the torque produced when the peroneal nerve was stimulated to cause a contraction of the anterior crural muscle. The maximum torque generated was normalized by the body mass of the mouse. Although there was no significant difference between the *Flt-1*$^{+/-}$ (101.0 ± 7.2) and the wild-type *Flt-1*$^{+/+}$ mice (100.3 ± 4.9), the *mdx:Flt-1*$^{+/-}$ mice (71.7 ± 4.3) generated more torque compared with the control *mdx:Flt-1*$^{+/+}$ mice (58.5 ± 4.7) (Fig. 6B). To evaluate systemic force production, whole-body tension analysis was conducted on the wild-type *Flt-1*$^{+/+}$, *Flt-1*$^{+/-}$, *mdx:Flt-1*$^{+/+}$ and *mdx:Flt-1*$^{+/-}$ mice. The *mdx:Flt-1*$^{+/-}$ mice showed an improvement in both maximum pulling force and average pulling force (maximum: 73.49 ± 4.85 and average: 63.47 ± 4.00) compared with the control *mdx:Flt-1*$^{+/+}$ mice (maximum: 62.83 ± 8.88 and average: 52.52 ± 6.74) (Fig. 6C and D). However, this improvement was only modest in comparison with the force produced by the wild-type *Flt-1*$^{+/+}$ mice.

Evaluation of *mdx:utrn*$^{-/-}$*:Flt-1*$^{+/-}$ triple-mutant mice

Although the *mdx* mice are genetically similar to DMD, they do not exhibit the pathology to the severity of DMD. Additionally, *mdx* mice show no significant difference in their lifespan compared with the wild-type mice. One of the reasons for the relatively mild phenotype of *mdx* mice is the upregulation of utrophin protein which can compensate for the lacking function of dystrophin. *mdx* mice carrying a *utrophin* gene mutation (*utrn*$^{-/-}$) display a more severe muscle phenotype than the *mdx* mice (23,30). These mice display a marked kyphosis and usually die within 5 months. Therefore, they serve as a better animal model for DMD. Since we found no difference in the amount of utrophin between *mdx:Flt-1*$^{+/-}$ and *mdx:Flt-1*$^{+/+}$ mice by western blotting (Fig. 3C and E), we proceeded to create triple-mutant *mdx:utrn*$^{-/-}$*:Flt-1*$^{+/-}$ and the control *mdx:utrn*$^{-/-}$*:Flt-1*$^{+/+}$ mice. *mdx:utrn*$^{-/-}$*:Flt-1*$^{+/-}$ mice were viable, and progenies were found to be

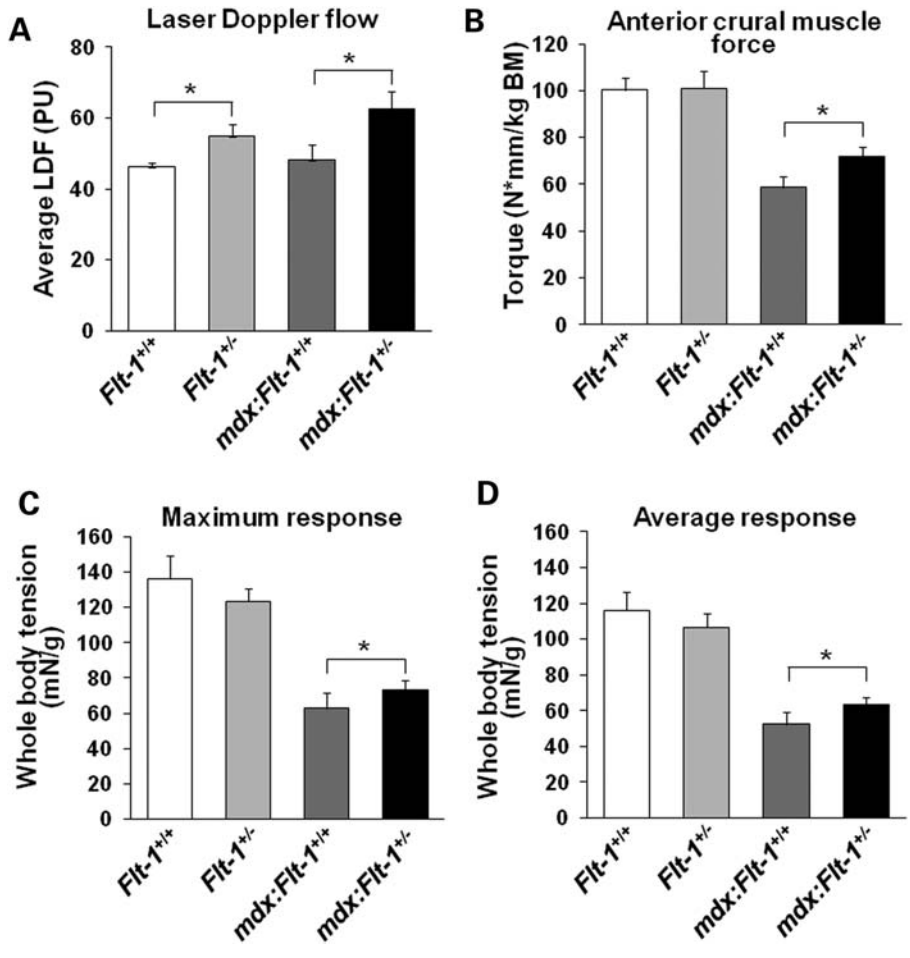

Figure 6. *mdx:Flt-1*$^{+/-}$ display improved blood flow and muscle function. (**A**) The *Flt*$^{+/-}$ and *mdx:Flt-1*$^{+/-}$ mice ($n = 5$ each) display increased amounts of blood flow as evaluated by LDF compared with the wild-type (*Flt-1*$^{+/+}$) and *mdx:Flt-1*$^{+/+}$ mice ($n = 8$ each). (**B**) The *Flt-1*$^{+/-}$ and wild-type (*Flt-1*$^{+/+}$) mice had no difference in the maximum isometric torque produced by the anterior crural muscles ($n = 5$ each). However, the *mdx:Flt-1*$^{+/-}$ mice had higher maximum isometric torque production compared with the *mdx:Flt-1*$^{+/+}$ mice ($n = 8$ each). (**C** and **D**) Whole-body tension assay shows that the *mdx:Flt-1*$^{+/-}$ mice ($n = 18$) had increased force production compared with the control *mdx:Flt-1*$^{+/+}$ mice ($n = 15$). There was no difference between the wild-type (*Flt-1*$^{+/+}$) and *Flt-1*$^{+/-}$ mice ($n = 5$ each). Values are mean $\pm$ SEM. Asterisks indicate experimental pairs where differences between the compared values were statistically significant ($P < 0.05$).

in the expected Mendelian ratio (data not shown). The loss of both the dystrophin and utrophin results in a very severe muscle phenotype with a very high fiber turnover. However, histological assessment of the TA muscle showed decreased amounts of CLN in the *mdx:utrn*$^{-/-}$*:Flt-1*$^{+/-}$ mice (73.28 ± 1.94) compared with the control *mdx:utrn*$^{-/-}$*:Flt-1*$^{+/+}$ (85.09 ± 1.99) littermates (Fig. 7A and B). The *mdx:utrn*$^{-/-}$*:Flt-1*$^{+/-}$ mice also displayed a significant increase in the body mass compared with the control *mdx:utrn*$^{-/-}$*:Flt-1*$^{+/+}$ mice (Fig. 7C).

Importantly, the average lifespan of *mdx:utrn*$^{-/-}$*:Flt-1*$^{+/-}$ mice was significantly extended (177.88 days $\pm$ 17.60) compared with the control *mdx:utrn*$^{-/-}$*:Flt-1*$^{+/+}$ mice (91.76 days $\pm$ 10.22) (Fig. 7D and E). Both genotypes are stable for around 30–50 days, after which the *mdx:utrn*$^{-/-}$*:Flt-1*$^{+/+}$ mice show a sharp decline in viability compared with a more gradual lethality seen in the *mdx:utrn*$^{-/-}$*:Flt-1*$^{+/-}$ mice. A Kaplan–Meier survival test showed there to be a significant difference between the two genotypes (Fig. 7D). These data strongly suggest that *Flt-1*$^{+/-}$ background attenuated the muscular dystrophy phenotype of the *mdx:utrn*$^{-/-}$ double-mutant mice to extend their lifespan, possibly through increased vascular density. Taken together, these data show that developmentally increasing angiogenesis and vascular density can partially rescue the dystrophic phenotype in DMD model mice.

No change in inflammatory response in the *mdx:Flt-1*$^{+/-}$ mice

Inflammation is known to contribute to muscle healing and regeneration. In addition, it is reported that Flt-1 is also expressed in macrophages (31). Therefore, we compared the degree of inflammation in the TA muscle isolated from the *mdx:Flt-1*$^{+/-}$ mice and the control *mdx:Flt-1*$^{+/+}$ mice. Immunostaining for Mac-1 (a marker for monocytes and macrophages) and Gr-1 (a marker for monocytes and granulocytes) showed there was no significant difference in the number of inflammatory cells that were observed in the TA muscle

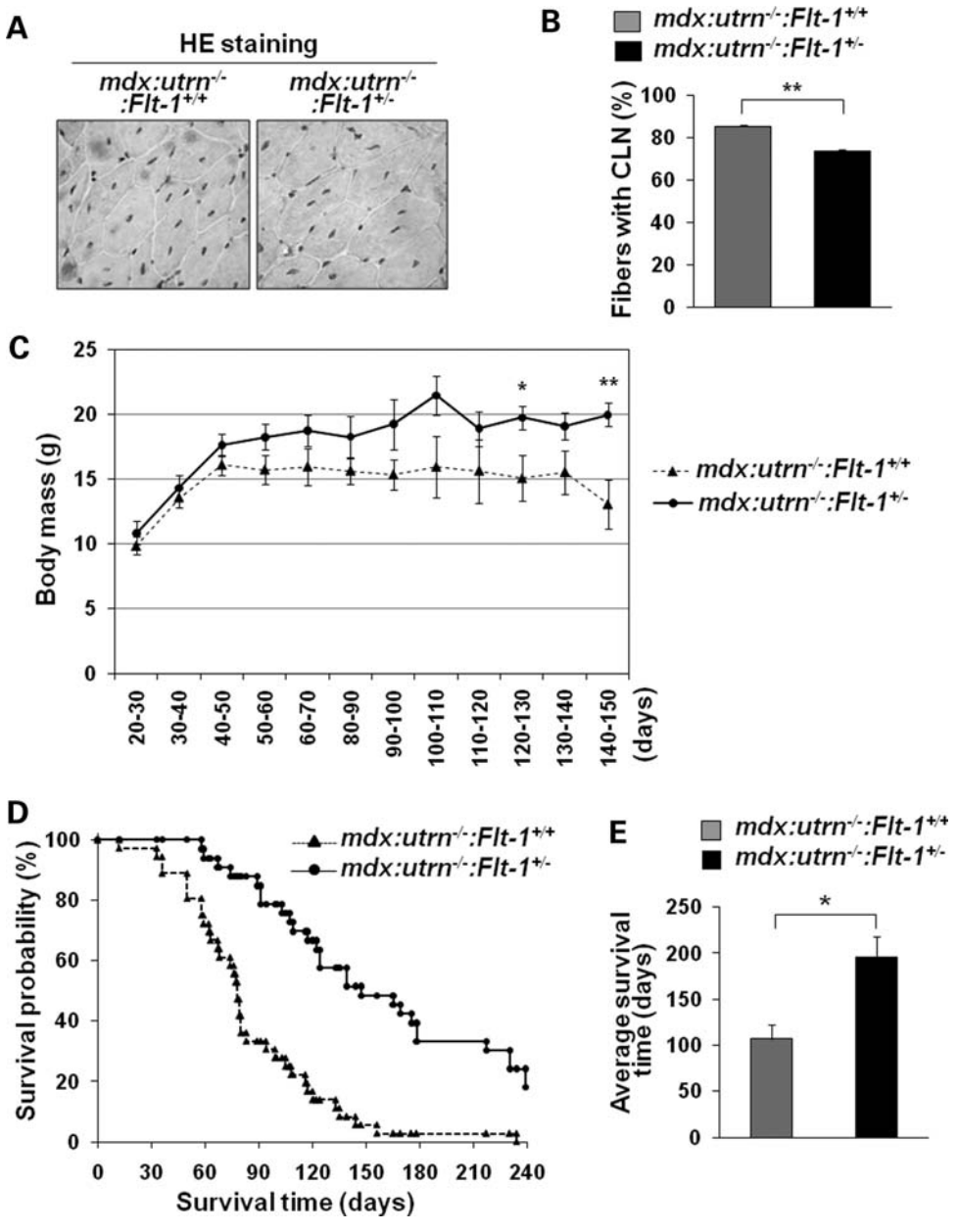

Figure 7. *mdx:utrn*$^{-/-}$*:Flt-1*$^{+/-}$ triple-mutant mice display an improved phenotype compared with the *mdx:utrn*$^{-/-}$*:Flt-1*$^{+/+}$ mice. (**A**) Representative images from HE staining of the TA muscle of the *mdx:utrn*$^{-/-}$*:Flt-1*$^{+/-}$ and the control *mdx:utrn*$^{-/-}$*:Flt-1*$^{+/+}$ mice. (**B**) The *mdx:utrn*$^{-/-}$*:Flt-1*$^{+/-}$ mice ($n = 6$) contain less muscle fibers with CLN compared with the *mdx:utrn*$^{-/-}$*:Flt-1*$^{+/+}$ mice ($n = 5$). (**C**) The *mdx:utrn*$^{-/-}$*:Flt*$^{+/-}$ mice ($n = 18$) show increased body mass compared with *mdx:utrn*$^{-/-}$*:Flt-1*$^{+/+}$ mice ($n = 20$). (**D**) A Kaplan–Meier survival test shows the *mdx:utrn*$^{-/-}$*:Flt-1*$^{+/-}$ mice ($n = 33$) have a longer survival probability and higher average survival time (**E**) compared with the *mdx:utrn*$^{-/-}$*:Flt-1*$^{+/+}$ mice ($n = 36$). Values are mean ± SEM. Asterisks or double asterisks indicate experimental pairs where differences between the compared values were statistically significant ($P < 0.05$ or $P < 0.01$, respectively).

between the *mdx:Flt-1*$^{+/-}$ mice and the control *mdx:Flt-1*$^{+/+}$ (Supplementary Material, Fig. S2).

Satellite cells are negative for VEGF receptors Flt-1 and Flk-1

Several reports have implicated that satellite cell proliferation and migration are influenced by VEGF, possibly through its receptors, Flk-1 and Flt-1 (15). To elucidate whether satellite cells express Flt-1 and Flk-1 and to examine for any potential cell autonomous effects, we first characterized lacZ expression in the TA muscle of *Flt*−1$^{+/-}$ (*Flt-1-lacZ*) (14), *Flk-1-lacZ* (32) and *Myf5*$^{+/\mathrm{nLacZ}}$ knock-in mice (33,34). These lacZ expressions recapitulate endogenous Flt-1, Flk-1 and Myf5 expression. Clearly, lacZ-positive cells were detected around vasculatures located outside of laminin-positive basal lamina of muscle fibers in both *Flt-1-lacZ* and *Flk-1-lacZ* mice (Supplementary Material, Fig. S3A). In contrast, lacZ-positive

satellite cells were detected within laminin-positive basal lamina of muscle fibers in *Myf5*$^{+/nLacZ}$ mice, indicating that quiescent satellite cells and muscle fibers do not express Flt-1 or Flk-1 (Supplementary Material, Fig. S3A). Next, we isolated single-muscle fibers from both *Flt-1-lacZ* and *Flk-1-lacZ* mice along with control *Myf5*$^{+/nLacZ}$ mice (Supplementary Material, Fig. S3B). As expected, the satellite cells started proliferating around day 2, and by day 5, a large amount of satellite cell-derived myoblasts had started dividing outside the muscle fibers (35). However, none of the cultures from *Flt-1-lacZ* or *Flk-1-lacZ* mice were stained positive for lacZ, indicating that neither quiescent satellite cells nor satellite cell-derived myoblasts express Flt-1 or Flk-1. In addition, none of the myotubes differentiated from myoblasts isolated from *Flt-1-lacZ* and *Flk-1-lacZ* mice were stained positive for lacZ. In contrast, satellite cells and satellite cell-derived myoblasts were clearly positive for lacZ in cultures from *Myf5*$^{+/nLacZ}$ mice. In addition, immunostaining clearly showed that desmin-positive myoblasts are negative for Flt-1 or Flk-1, whereas human umbilical vein endothelial cells (HUVECs) are positive for both receptors (Supplementary Material, Fig. S3C). Therefore, these results strongly indicated that non-cell autonomous effects improved muscle phenotype in the *mdx:Flt-1*$^{+/-}$ mice.

Increased proliferation of myogenic precursor cells by increased vascular niche

The single-muscle fiber experiments ruled out the possibility that heterozygous *Flt-1* gene knockout cell autonomously affects satellite cell-derived myogenic precursor cell proliferation or differentiation. The muscle in *mdx* mice is able to regenerate effectively in early stages due to the proliferation of the satellite cell pool, which fuses with the existing muscle fibers to repair the damaged tissue. However, as the muscle ages, the satellite cell number decreases, resulting in impaired muscle regeneration (28). To examine whether the number of satellite cells and myogenic precursor cells was affected in the *mdx:Flt-1*$^{+/-}$ mice compared with the control *mdx:Flt-1*$^{+/+}$ mice, we performed FACS analysis on dissociated cells from the TA muscle and characterized them using a satellite cell-specific antibody, SM/C-2.6 (36) (Fig. 8A and B). Interestingly, although the total number of SM/C-2.6^{+} satellite cells and myogenic precursor cells isolated from the TA muscle of *Flt-1*$^{+/-}$ mice showed no significant difference compared with those of the wild-type *Flt-1*$^{+/+}$ mice, these cell populations were markedly increased in the *mdx:Flt-1*$^{+/-}$ mice compared with the control *mdx:Flt-1*$^{+/+}$ mice. The increased number of Pax7 $^{+}$ satellite cells located underneath basal lamina (laminin^{+}) in the *mdx:Flt-1*$^{+/-}$ mice were also detected in TA muscle sections (Fig. 8C and D). Therefore, it is possible that increased vascular niche might promote myogenic precursor cell proliferation and/or survival.

To test for possible interaction between endothelial cells and myogenic precursor cells, satellite cell-derived primary myoblasts were cultured by themselves or co-cultured with either mouse 10T1/2 fibroblasts or mouse brain-derived endothelial (b.End3) cell lines (Fig. 8E and F). The cells were grown in myoblast growth media for 3 days and then stained for the muscle marker desmin. Myoblasts co-cultured with b.End3 cells displayed more desmin-positive cells than myoblasts alone or myoblasts co-cultured with 10T1/2 cells, indicating that co-culture with endothelial cells but not with fibroblasts promotes myoblast proliferation and/or survival. Taken together, these results strongly suggest that the increased levels of endothelial cells seen in *mdx:Flt-1*$^{+/-}$ muscle and the associated increased vascular niche may promote satellite cell-derived myogenic precursor cell proliferation. It is likely that this occurs by secreted factors from endothelial cells or direct interaction between endothelial cells and satellite cells or myogenic precursor cells. This may be important for the suppression of fibrosis and calcification along with the protection of muscle damage in dystrophic muscle, thus improving muscle contractile function.

DISCUSSION

Although there is currently no effective therapeutic options for DMD, there are many promising active areas of research (37,38). Most of these options focus on repairing the mechanoinstability of the muscle through cell therapy, gene therapy or a combination of the two. Recently, it has been shown that alleviating the problems associated with vasculature seen in *mdx* mice can drastically improve the diseased phenotype in *mdx* mice (5,12,19). However, the developmental relationship between angiogenesis and muscular dystrophy phenotype has remained to be elucidated.

In this report, we sought to compensate for the functional ischemia in the muscle of DMD model mice by developmentally increasing the vascular density. We found that the *Flt-1*$^{+/-}$ mice as well as the *mdx:Flt-1*$^{+/-}$ mice show increased blood vessel density in the muscle compared with the control *Flt-1*$^{+/+}$ or *mdx:Flt-1*$^{+/+}$ mouse counterparts. The increase in blood vessel density translates to an increase in blood perfusion to the muscle and better histological muscle phenotype as improved muscle contractile function. Concomitantly, it also led to an increase in survival rates and to improvement of muscle histology in the *mdx:utrn*$^{-/-}$*:Flt-1*$^{+/-}$ combined triple-mutant mice compared with the control *mdx:utrn*$^{-/-}$*:Flt-1*$^{+/+}$ double-mutant mice. To our knowledge, this study is the first showing that developmentally increasing angiogenesis and thereby increasing vascular density can partially rescue the dystrophic phenotype in DMD model mice. Potential mechanisms include (i) decreased inflammatory response, (ii) cell autonomous effects, (iii) reducing ischemia by increasing tissue perfusion or (iv) increased vascular-derived interaction to increase satellite cell proliferation and/or protect muscle damage.

It is reported that to make room for new muscle fiber, muscle damage is followed by recruitment of macrophages to clear away the cellular debris left by damaged muscle tissue (39–42). However, we found no significant difference in the numbers of Mac-1^{+}- or Gr-1^{+}-infiltrated cells in the muscle of *mdx:Flt-1*$^{+/-}$ compared with the control *mdx:Flt-1*$^{+/+}$ mice. Several reports have shown that VEGF has an effect on muscle satellite cell-derived myogenic precursor cells for cell proliferation and survival, mediated through its two major receptors, Flt-1 and Flk-1 (35,43). Since our

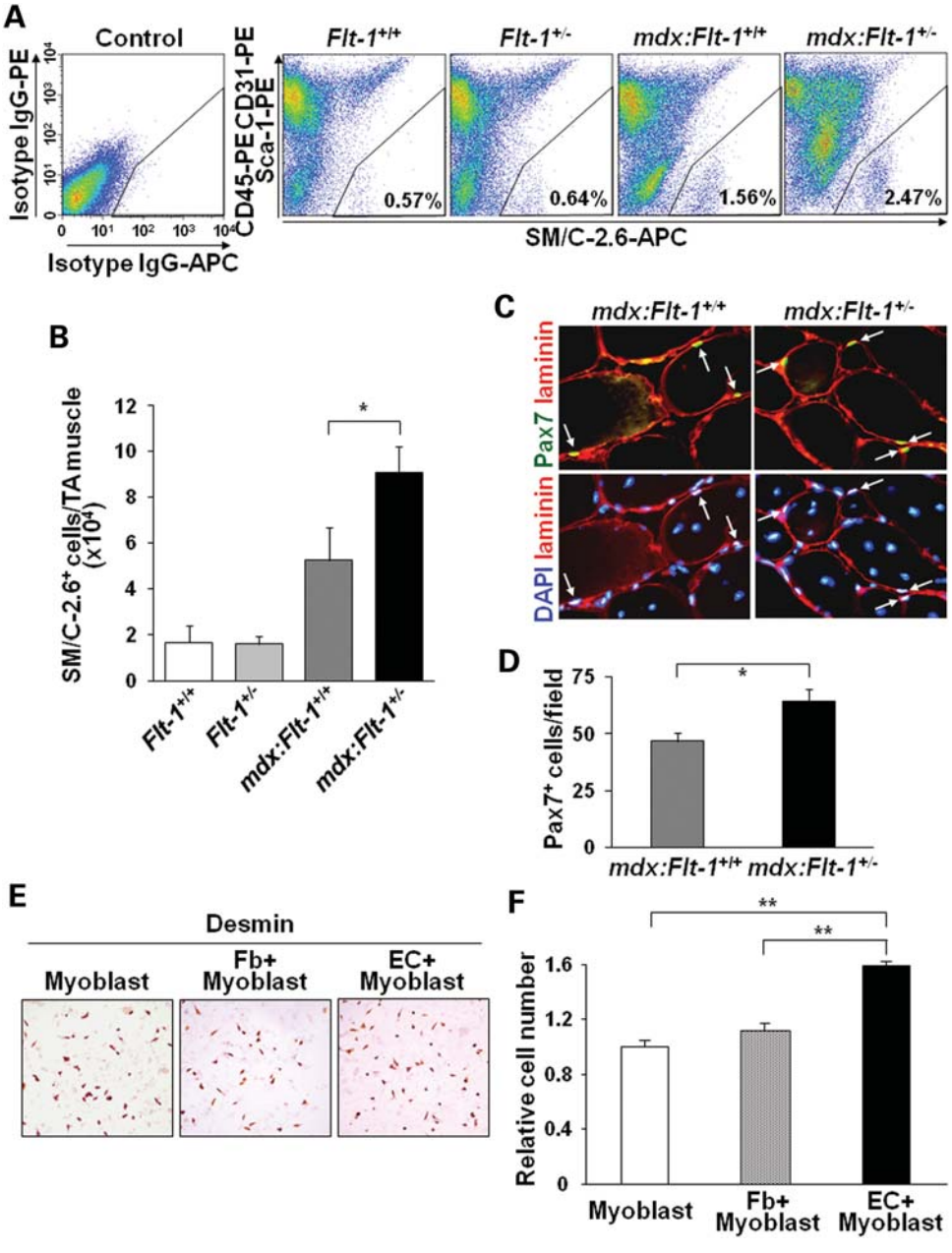

Figure 8. Increased myogenic cells in the increased vascular niche. (**A**) FACS analysis shows that the dissociated cells from the TA muscle of the *mdx:Flt-1*$^{+/-}$ mice contained increased amount of CD45-PE$^-$ CD31-PE$^-$ Sca-1-PE$^-$ SM/C-2.6-APC$^+$ satellite cells and myogenic precursor cells in the gated areas, compared with the *mdx:Flt-1*$^{+/+}$ mice. Control indicates the FACS profile for the control antibodies. (**B**) Total number of CD45$^-$ CD31$^-$ Sca-1$^-$ SM/C-2.6$^+$ myogenic cells per TA muscle was estimated by multiplying the percent from the FACS analysis ($n = 6$ each) with the total number of cells obtained from the TA muscle. (**C**) Representative images from TA muscle sections of the control *mdx:Flt-1*$^{+/+}$ and *mdx:Flt-1*$^{+/-}$ mice stained with anti-Pax7 antibody (green) to detect satellite cells (arrows) and anti-laminin antibody (red) to detect basal lamina. Nuclei were counterstained with DAPI (blue). (**D**) Quantification of Pax7$^+$ myogenic cells in a TA muscle of the control *mdx:Flt-1*$^{+/+}$ ($n = 4$) and *mdx:Flt-1*$^{+/-}$ ($n = 3$) mice. Relative amount of Pax7$^+$ cells counted in a view field. (**E**) Desmin staining on myoblast co-culture with fibroblasts (10T1/2) cell line (Fb) or endothelial (b.End3) cell line (EC). (**F**) Quantification of the proliferation of myoblast as evaluated by the number of desmin-positive cells in culture ($n = 3$ each). Values are mean ± SEM. Asterisks or double asterisks indicate experimental pairs where differences between the compared values were statistically significant ($P < 0.05$ or $P < 0.01$, respectively).

system modulates the expression of Flt-1, it is important to examine cell autonomous effect on the muscle fibers and myogenic precursor cells. First, the muscle sectioning demonstrated that Flt-1- or Flk-1-expressing cells are located outside of basal lamina of muscle fibers. We also chose to examine the expression in satellite cell and satellite cell-derived myoblasts by single-muscle fiber cultures since it is possible to obtain the purest satellite cell population using this method. By immunological detection and *lacZ* knock-in mice, our data clearly demonstrate that muscle fibers, satellite cells and satellite cell-derived myoblasts do not express Flt-1 and Flk-1. This suggests that there are no cell autonomous effects on the muscle fibers or myogenic precursor cells through these receptors in our system.

Importantly, the increase in the blood vessel density in the *Flt-1*$^{+/-}$ and *mdx:Flt-1*$^{+/-}$ mice also translated into an increase in LDF at rest. During rest, the skeletal muscle lacks complete perfusion due to the absence of complete recruitment of the microvasculature (44). This recruitment of the microvasculature has been examined during exercise as well as during insulin infusion. During muscle activity, NOS-mediated vasodilation can increase the passive pressure gradient in the capillary beds, thereby recruiting more microvasculature and increasing tissue perfusion (45,46). The ischemic state created due to the lack of such vasodilation during contraction is a direct cause of muscle fiber damage *in vivo* in *mdx* mice (12). Therefore, the increase in basal blood flow detected in our muscular dystrophy model mice may offer a protective mechanism for the contraction-induced damage seen in the DMD (43).

Increased endothelial cell production in the muscle can have many different beneficial effects on dystrophic muscle through paracrine stimulation by protecting muscle fiber damage and activating myogenic precursor cells as a vascular niche. Numerous reports have shown cross-talk between endothelial cells and satellite cells (19,47,48). Our results as well as others have shown that endothelial cells and factors produced by them can mediate the response on satellite cell survival and proliferation (18,47,48). This is in accordance to our co-culture experiments which show increased proliferation of satellite cell-derived myoblasts when co-cultured with endothelial cells. Recently, Christov *et al*. (47) have shown that satellite cells are preferentially located next to capillaries. Since our model increases the amount of capillaries found in the muscle, it may effectively increase the amount of vascular niches that house the satellite cell compartment in the muscle. In this report we show that the number of satellite cells and myogenic precursor cells is markedly increased in the *mdx:Flt-1*$^{+/-}$ mice compared with the control *mdx:Flt-1*$^{+/+}$ mice. This increase in the number of satellite cells and myogenic precursor cells may be responsible for the improved phenotype seen in the *mdx:Flt-1*$^{+/-}$ mice.

The present study shows that increased angiogenesis may be a novel avenue to improve some of the dystropathologies and functional parameters associated with DMD that can be used in conjuncture with other treatment strategies. For example, intramuscular injection of VEGF-containing recombinant adeno-associated viral vectors has been shown to make both functional and histological improvements in the both ischemic muscle and *mdx* muscle (19,49,50). This improvement is seen in combination with an increase in angiogenesis in the muscle. Ito *et al*. (5) also showed the importance of the lack of dystrophin in the vascular smooth muscle. They showed that expression of smooth-muscle-specific dystrophin in *mdx* mice resulted in partially improved muscle phenotype.

It is important to understand how vasculatures interact with muscle fibers and muscle stem cells to provide necessary oxygen and nutrition, protect from cell death and provide a vascular niche. Further studies are required to ascertain the exact mechanism and the long-term effects of increasing the vasculature. From a therapeutic point of view, neovascularization could be induced in dystrophic muscle using the administration of angiogenic factors, such as VEGF protein (19,49,50).

MATERIALS AND METHODS

Animals

DMD model *mdx-5cv* mice (B6Ros.Cg-*Dmd*$^{mdx\text{-}5Cv}$/J) were obtained from the Jackson Laboratory (22). Heterozygous *Flt-1* gene knockout (*Flt-1*$^{+/-}$ or *Flt-1-lacZ*) (13), *Flk-1-lacZ* (32) and *Myf5*$^{+/nLacZ}$ (33) knock-in mice were provided by Drs Guo-Hua Fong, Masatsugu Ema and Shahragim Tajbakhsh, respectively. *mdx-5cv:Flt-1*$^{+/-}$ (double-mutant) mice and *mdx−5cv:Flt-1*$^{+/+}$ (control) mice were established by crossing *mdx-5cv* with *Flt-1*$^{+/-}$ mice. Heterozygous knockout mice for the *utrophin*$^{+/-}$ (*utrn*$^{+/-}$) mice were obtained from Dr Robert W. Grange (30). *mdx-5cv:utrn*$^{-/-}$*:Flt-1*$^{+/-}$ (triple-mutant) mice and *mdx-5cv:utrn*$^{-/-}$*:Flt-1*$^{+/+}$ (control) mice were established by crossing *mdx-5cv:Flt-1*$^{+/-}$ with *utrn*$^{+/-}$ mice. Age-matched litter mate mice (2–3 months old) were examined for experiments. Genotyping to detect the mutated alleles of *mdx-5cv* and *utrophin* was performed by PCR using the following primers: For *mdx-5cv* forward primer (no. 0981), 5′-GAAGCTCCCAGAGACAAGTC-3′; and reverse primer (no. 0982), 5′-TCATGAGCATGAAACTGTTCTT-3′. The PCR product DNA was digested with *Dra*III restriction enzyme (New England Biolabs). Wild-type allele generated 180 bp and mutant allele generated 50 and 130 bp bands. For the genotyping of *utrophin*, forward primer for *utrophin* knockout (no. 22803), 5′-TGCCAAGTTCTAATT CCATCAGAAGCTG-3′; forward primer for wild-type *utrophin* (no. 553), 5′-TGCAGTGTCTCCCAATAAGGTATGAAC-3′; and a common reverse primer (no. 554), 5′-CTG AGTCAAACAGCTTGGAAGCCTCC-3. For the genotyping of *Flt-1*$^{+/-}$ (*Flt-1-lacZ*), *Flk-1-lacZ* and *Myf5*$^{+/nLacZ}$ mice, small pieces of ear or tail tissue were stained with X-gal (Sigma-Aldrich) solution for lacZ expression as described previously (51). The animals were housed in an SPF environment and were monitored by the Research Animal Resources (RAR) of the University of Minnesota. All protocols were approved by the Institutional Animal Care and Usage Committee (IACUC) of the University of Minnesota.

Histological analysis

Freshly dissected tissues were embedded and frozen in OCT tissue freezing medium (Fisher Scientific) and sectioned at 8 μm thickness by cryostat. Sections were routinely stained with hematoxlyn and eosin (HE), and age-matched samples were used to quantify both CLN and fiber diameter. Sections were also stained with Alizarin red (Sigma-Aldrich), Oil red O (Sigma-Aldrich), van Gieson (elastic stain kit: Sigma-Aldrich) and NADH-TR (Sigma-Aldrich) for the assessment of calcification, adipose, fibrosis and fiber type, respectively. To access membrane permeability, EBD was used as described previously (24,25). Briefly, a solution of 1% Evans blue (Fluka), 0.1 ml/10 g of body mass, was injected in the intraperitoneal cavity. After 16–20 h, the animals were euthanized and their tissues were harvested. All analysis was performed manually using the ImageJ software from the NIH (52).

Immunostaining

Eight micron thick transverse cryosections were used with the Vectastain Elite ABC Kit (Vector Laboratories) for immunohistochemistry according to the manufacturer's instructions. Sections were labeled with anti-CD31 (eBioscience) followed by biotin-conjugated anti-mouse IgG secondary antibody. Sections were also labeled with biotin-conjugated anti-Mac-1 (eBioscience) and biotin-conjugated anti-Gr-1 antibodies (eBioscience). Sections were colorized using 3-amino-9-ethylcarbazole (AEC) (Sigma-Aldrich). Sections were also labeled using anti-slow MHC antibody (Sigma-Aldrich), anti-dystrophin antibody (Sigma-Aldrich) or anti-Pax7 antibody (R & D Systems) and anti-laminin antibody (Sigma-Aldrich) followed by Alexa 488-conjugated anti-mouse IgG and Alexa 596-conjugated anti-rabbit IgG secondary antibodies. Cell cultures were stained with anti-desmin antibody (Dako: D33), anti-Flt-1 antibody (Santa Cruz) or anti-Flk-1 antibody (BD Biosciences), followed by Alexa 488-conjugated anti-mouse IgG, Alexa 488-conjugated anti-goat IgG, Alexa 488-conjugated anti-rat IgG secondary antibody, respectively. Cell cultures were also stained by the Vectastain Elite ABC Kit, followed by AEC. LacZ expression in muscle was detected by X-gal staining overnight as described previously (51). Anti-laminin antibody (Sigma-Aldrich) was used to detect muscle basal lamina in X--gal-stained muscle sections. Sections and cell cultures were also nuclear stained with DAPI (4′,6-diamidino-2-phenylindole) (Sigma-Aldrich) and mounted with Dako fluorescence mounting media (Dako). Microscopic images were captured by a DP-1 digital camera attached to BX51 fluorescence microscope with 20× and 40× UPlanFLN objectives (all from Olympus). Photoshop C2 (Adobe Systems) was used for image processing.

In vivo force measurements

Maximal isometric torque of the hind limb dorsiflexors was assessed as described previously (53). Briefly, mice were anesthetized with a cocktail of fentanyl citrate (10 mg/kg body weight), droperidol (0.2 mg/kg body weight) and diazepam (5 mg/kg body weight). The left hind limb was then shaved, aseptically prepared, and each mouse was positioned on a heated platform, with its left foot placed in a metal foot plate attached to the shaft of a servomotor (model 300B-LR, Aurora Scientific, Aurora, Ontario, Canada). Two platinum electrodes (model E2-12, Grass Technologies, West Warwick, RI, USA) were inserted subcutaneously on either side of the peroneal nerve. A stimulator and stimulus isolation unit (models S48 and SIU5, respectively, Grass Technologies) stimulated the peroneal nerve via the platinum electrodes to induce a contraction of the anterior crural muscles. The parameters for stimulation were set at a 200 ms contraction duration consisting of 0.5 ms square-wave pulses at 300 Hz. The voltage was adjusted from 3.0 to 9.0 v until maximal isometric torque was achieved. Isometric torque results are presented per kilogram of body mass.

Whole-body tension assay

Muscle force production was measured by the whole-body 'escape' test as reported previously (54). Wild-type *Flt-1*$^{+/+}$, *Flt-1*$^{+/-}$, *mdx:Flt-1*$^{+/+}$ and *mdx:Flt-1*$^{+/-}$ mice were placed between parallel wooden barriers to allow for forward movement only. The tails were attached to a fixed range force transducer (BioPac Systems). They were given a light pinch every 15 s and the force was measured for 5 min. The force values were normalized against the mouse body mass.

Laser Doppler flow

RBC flux was evaluated using the moorLab^{TM} LDF meter with the MP7a probe that allows for collecting light from a deeper tissue level than standard probes according to the manufacturer's instructions (Moor Instruments, Millwey, Axminster, UK) (55). The fur from the right hind leg was removed using a chemical depilatory. Readings were taken using the probe from at least 10 different spots on the TA muscle. The PU was determined as the mean PU-value of the stabilized plateau.

Fluorescence-activated cell sorting

Dissociated cells were prepared from the TA muscle of 2-month-old mice after digestion of the muscle with collagenase type B and dispase II (Roche Diagnostics) (56). FACS analysis was performed on a FACS caliber equipped with double lasers (BD Biosciences). The following antibodies were used for FACS analysis: SM/C-2.6, kindly provided by Dr S. Fukada (36) with Alexa 488-labeled anti-mouse IgG, allophycocyanin (APC)-labeled CD31, phycoerythrin (PE)-labeled CD31, PE-labeled CD45, PE-labeled Sca-1 (all from PharMingen). Mouse and rat normal IgG conjugated with APC, PE and FITC (PharMingen) were used in the control experiment. Alexa 488/FITC and PE were excited by a 488 nm argon laser and their fluorescence was detected with an FL1 (530/30) and an FL2 (576/26) filter, respectively. APC was excited by a 633 nm red diode laser for the detection with an FL4 filter (620/20). Gates were strictly defined on the basis of single-antibody-stained control cells, as well as the forward scatter and side scatter patterns of the cells.

Single-muscle fiber culture

Single-muscle fibers were isolated from extensor digitorum longus (EDL) muscle of *Flt-1-lacZ*, *Flk-1-lacZ* and *Myf5*$^{+/nLacZ}$ mice, as reported previously (34,35). EDL muscle was dissected tendon to tendon. The dissected muscle was incubated in 0.2% collagenase type I (Sigma-Aldrich) at 37°C for 45–60 min. Heat-polished pipettes of subsequently smaller bore sizes were used gently to triturate and release the muscle fibers. Single-muscle fibers were picked up and transferred to Matrigel (BD Biosciences)-coated plates. The culture was maintained for up to 5 days at 37°C and 5% CO_2 incubator. Plates were fixed for X-gal staining at appropriate time intervals, as reported previously (57).

Cell culture

Satellite cell-derived primary myoblasts were isolated from adult lower hind limb muscle from 2-month-old mice as described previously (58,59). Cells were maintained on

collagen-coated dishes in myoblast growth medium consisting of HAM's F-10 medium supplemented with 20% FBS and 10 ng/ml basic FGF (R&D Systems). C3H10T1/2 fibroblast cell line and b.End3 cells were obtained from ATCC and maintained in DME medium supplemented with 10% FBS. Human umbilical vein endothelial cells (HUVEC) were kindly obtained from Dr Gregory M. Vercellotti and maintained on 1% gelatin-coated dishes in medium 199 supplemented with 10% FBS. Myoblasts were co-cultured with equal numbers of either 10T1/2 cells or b.End3 cells in myoblast growth medium. Myoblast proliferation was quantified by a number of desmin-positive cells 3 days after co-culture. At least 100 desmin-positive myoblasts were counted for each experiment.

Western blotting

Muscle proteins were isolated following the previously published protocols (60). The protein concentration of the fractions was determined by Micro BCA Protein Assay Reagent Kit (Pierce). Utrophin and dystrophin proteins were detected by western blotting with anti-utrophin antibody (Developmental Study Hybridoma Bank), or anti-dystrophin antibody (Sigma-Aldrich), followed by anti-mouse IgG-HRP (Bio-Rad). To verify equal loading proteins, the same blots were stripped and re-probed with anti-β-tubulin antibody (Sigma-Aldrich), followed by anti-mouse IgG-HRP (Bio-Rad). The reaction was developed using SuperSignal West Femto chemiluminescent substrate (Pierce) in accordance with the manufacturer's instructions.

Statistics

All data are presented as mean ± SEM. Comparison between groups was done by Student's *t*-test using a two-tailed distribution with two-sample equal variance unless otherwise stated. Data were considered statistically significant at $P < 0.05$. $^{*}P < 0.05$ and $^{**}P < 0.01$.

SUPPLEMENTARY MATERIAL

Supplementary Material is available at *HMG* online.

ACKNOWLEDGEMENTS

The authors would like to thank Drs James Ervasti and Kurt Prins for technical assistance in the whole-body tension assay and constructive comments, Dr LaDora V. Thompson for technical assistance in the western blotting, Dr Walter Low for the use of the MoorLab Laser Doppler, Dr Gregory M. Vercellotti for providing HUVECs, Dr So-ichiro Fukada for providing SM/C-2.6 antibody, Dr Robert W. Grange for providing *mdx:utrn*$^{+/-}$ mice and Dr Shahragim Tajbakhsh for providing *Myf5*$^{+/\mathrm{nLacZ}}$ mice. FACS analysis was performed in the flow cytometry facility of the Stem Cell Institute, University of Minnesota Medical School.

Conflict of Interest statement. None declared.

FUNDING

This work was supported by the Undergraduate Research Opportunity Program (637-5904 to M.V.); the Gregory Marzolf Muscular Dystrophy Training Grant (06378016 to M.V.); NIH P30 grant (P30AR057220 to D.A.L.) for supplying the *mdx:utrn*$^{-/-}$ mice, and the Muscular Dystrophy Association (MDA69856 to A.A.).

REFERENCES

1. Dalkilic, I. and Kunkel, L.M. (2003) Muscular dystrophies: genes to pathogenesis. *Curr. Opin. Genet. Dev.*, **13**, 231–238.
2. Davies, K.E. and Nowak, K.J. (2006) Molecular mechanisms of muscular dystrophies: old and new players. *Nat. Rev. Mol. Cell Biol.*, **7**, 762–773.
3. Mendell, J.R., Engel, W.K. and Derrer, E.C. (1971) Duchenne muscular dystrophy: functional ischemia reproduces its characteristic lesions. *Science*, **172**, 1143–1145.
4. Miyatake, M., Miike, T., Zhao, J., Yoshioka, K., Uchino, M. and Usuku, G. (1989) Possible systemic smooth muscle layer dysfunction due to a deficiency of dystrophin in duchenne muscular dystrophy. *J. Neurol. Sci.*, **93**, 11–17.
5. Ito, K., Kimura, S., Ozasa, S., Matsukura, M., Ikezawa, M., Yoshioka, K., Ueno, H., Suzuki, M., Araki, K., Yamamura, K. *et al.* (2006) Smooth muscle-specific dystrophin expression improves aberrant vasoregulation in mdx mice. *Hum. Mol. Genet.*, **15**, 2266–2275.
6. Cullen, M.J. and Jaros, E. (1988) Ultrastructure of the skeletal muscle in the X chromosome-linked dystrophic (mdx) mouse: comparison with duchenne muscular dystrophy. *Acta Neuropathol.*, **77**, 69–81.
7. Loufrani, L., Levy, B.I. and Henrion, D. (2002) Defect in microvascular adaptation to chronic changes in blood flow in mice lacking the gene encoding for dystrophin. *Circ. Res.*, **91**, 1183–1189.
8. Loufrani, L., Matrougui, K., Gorny, D., Duriez, M., Blanc, I., Levy, B.I. and Henrion, D. (2001) Flow (shear stress)-induced endothelium-dependent dilation is altered in mice lacking the gene encoding for dystrophin. *Circulation*, **103**, 864–870.
9. Weir, A.P., Burton, E.A., Harrod, G. and Davies, K.E. (2002) A- and B-utrophin have different expression patterns and are differentially up-regulated in mdx muscle. *J. Biol. Chem.*, **277**, 45285–45290.
10. Coral-Vazquez, R., Cohn, R.D., Moore, S.A., Hill, J.A., Weiss, R.M., Davisson, R.L., Straub, V., Barresi, R., Bansal, D., Hrstka, R.F. *et al.* (1999) Disruption of the sarcoglycan–sarcospan complex in vascular smooth muscle: a novel mechanism for cardiomyopathy and muscular dystrophy. *Cell*, **98**, 465–474.
11. Rando, T.A. (2001) Role of nitric oxide in the pathogenesis of muscular dystrophies: a 'two hit' hypothesis of the cause of muscle necrosis. *Microsc. Res. Tech.*, **55**, 223–235.
12. Asai, A., Sahani, N., Kaneki, M., Ouchi, Y., Martyn, J.A. and Yasuhara, S.E. (2007) Primary role of functional ischemia, quantitative evidence for the two-hit mechanism, and phosphodiesterase-5 inhibitor therapy in mouse muscular dystrophy. *PLoS ONE*, **2**, e806.
13. Fong, G.H., Rossant, J., Gertsenstein, M. and Breitman, M.L. (1995) Role of the flt-1 receptor tyrosine kinase in regulating the assembly of vascular endothelium. *Nature*, **376**, 66–70.
14. Fong, G.H., Zhang, L., Bryce, D.M. and Peng, J. (1999) Increased hemangioblast commitment, not vascular disorganization, is the primary defect in flt-1 knock-out mice. *Development*, **126**, 3015–3025.
15. Ferrara, N., Gerber, H.P. and LeCouter, J. (2003) The biology of VEGF and its receptors. *Nat. Med.*, **9**, 669–676.
16. Kearney, J.B., Ambler, C.A., Monaco, K.A., Johnson, N., Rapoport, R.G. and Bautch, V.L. (2002) Vascular endothelial growth factor receptor flt-1 negatively regulates developmental blood vessel formation by modulating endothelial cell division. *Blood*, **99**, 2397–2407.
17. Springer, M.L., Ozawa, C.R., Banfi, A., Kraft, P.E., Ip, T.K., Brazelton, T.R. and Blau, H.M. (2003) Localized arteriole formation directly adjacent to the site of VEGF-induced angiogenesis in muscle. *Mol. Ther.*, **7**, 441–449.
18. Arsic, N., Zacchigna, S., Zentilin, L., Ramirez-Correa, G., Pattarini, L., Salvi, A., Sinagra, G. and Giacca, M. (2004) Vascular endothelial growth factor stimulates skeletal muscle regeneration *in vivo*. *Mol. Ther.*, **10**, 844–854.
19. Messina, S., Mazzeo, A., Bitto, A., Aguennouz, M., Migliorato, A., De Pasquale, M.G., Minutoli, L., Altavilla, D., Zentilin, L., Giacca, M. *et al.*

(2007) VEGF overexpression via adeno-associated virus gene transfer promotes skeletal muscle regeneration and enhances muscle function in mdx mice. *FASEB J.*, **21**, 3737–3746.
20. Coulton, G.R., Curtin, N.A., Morgan, J.E. and Partridge, T.A. (1988) The mdx mouse skeletal muscle myopathy. II. Contractile properties. *Neuropathol. Appl. Neurobiol.*, **14**, 299–314.
21. Coulton, G.R., Morgan, J.E., Partridge, T.A. and Sloper, J.C. (1988) The mdx mouse skeletal muscle myopathy. I. A histological, morphometric and biochemical investigation. *Neuropathol. Appl. Neurobiol.*, **14**, 53–70.
22. Danko, I., Chapman, V. and Wolff, J.A. (1992) The frequency of revertants in mdx mouse genetic models for Duchenne muscular dystrophy. *Pediatr. Res.*, **32**, 128–131.
23. Deconinck, A.E., Rafael, J.A., Skinner, J.A., Brown, S.C., Potter, A.C., Metzinger, L., Watt, D.J., Dickson, J.G., Tinsley, J.M. and Davies, K.E. (1997) Utrophin-dystrophin-deficient mice as a model for Duchenne muscular dystrophy. *Cell*, **90**, 717–727.
24. Matsuda, R., Nishikawa, A. and Tanaka, H. (1995) Visualization of dystrophic muscle fibers in mdx mouse by vital staining with Evans blue: evidence of apoptosis in dystrophin-deficient muscle. *J. Biochem. (Tokyo)*, **118**, 959–964.
25. Hamer, P.W., McGeachie, J.M., Davies, M.J. and Grounds, M.D. (2002) Evans blue dye as an *in vivo* marker of myofibre damage: optimising parameters for detecting initial myofibre membrane permeability. *J. Anat.*, **200**, 69–79.
26. Suelves, M., Vidal, B., Serrano, A.L., Tjwa, M., Roma, J., Lopez-Alemany, R., Luttun, A., de Lagran, M.M., Diaz-Ramos, A., Jardi, M. *et al.* (2007) uPA deficiency exacerbates muscular dystrophy in MDX mice. *J. Cell Biol.*, **178**, 1039–1051.
27. Pastoret, C. and Sebille, A. (1995) Mdx mice show progressive weakness and muscle deterioration with age. *J. Neurol. Sci.*, **129**, 97–105.
28. Brack, A.S., Bildsoe, H. and Hughes, S.M. (2005) Evidence that satellite cell decrement contributes to preferential decline in nuclear number from large fibres during murine age-related muscle atrophy. *J. Cell. Sci.*, **118**, 4813–4821.
29. Maggs, A.M., Taylor-Harris, P., Peckham, M. and Hughes, S.M. (2000) Evidence for differential post-translational modifications of slow myosin heavy chain during murine skeletal muscle development. *J. Muscle Res. Cell. Motil.*, **21**, 101–113.
30. Grady, R.M., Teng, H., Nichol, M.C., Cunningham, J.C., Wilkinson, R.S. and Sanes, J.R. (1997) Skeletal and cardiac myopathies in mice lacking utrophin and dystrophin: a model for Duchenne muscular dystrophy. *Cell*, **90**, 729–738.
31. Sawano, A., Iwai, S., Sakurai, Y., Ito, M., Shitara, K., Nakahata, T. and Shibuya, M. (2001) Flt-1, vascular endothelial growth factor receptor 1, is a novel cell surface marker for the lineage of monocyte-macrophages in humans. *Blood*, **97**, 785–791.
32. Ema, M., Takahashi, S. and Rossant, J. (2006) Deletion of the selection cassette, but not cis-acting elements, in targeted Flk1-lacZ allele reveals Flk1 expression in multipotent mesodermal progenitors. *Blood*, **107**, 111–117.
33. Tajbakhsh, S., Rocancourt, D. and Buckingham, M. (1996) Muscle progenitor cells failing to respond to positional cues adopt non-myogenic fates in myf-5 null mice. *Nature*, **384**, 266–270.
34. Beauchamp, J.R., Heslop, L., Yu, D.S., Tajbakhsh, S., Kelly, R.G., Wernig, A., Buckingham, M.E., Partridge, T.A. and Zammit, P.S. (2000) Expression of CD34 and Myf5 defines the majority of quiescent adult skeletal muscle satellite cells. *J. Cell Biol.*, **151**, 1221–1234.
35. Shefer, G. and Yablonka-Reuveni, Z. (2005) Isolation and culture of skeletal muscle myofibers as a means to analyze satellite cells. *Methods Mol. Biol.*, **290**, 281–304.
36. Fukada, S., Higuchi, S., Segawa, M., Koda, K., Yamamoto, Y., Tsujikawa, K., Kohama, Y., Uezumi, A., Imamura, M., Miyagoe-Suzuki, Y. *et al.* (2004) Purification and cell-surface marker characterization of quiescent satellite cells from murine skeletal muscle by a novel monoclonal antibody. *Exp. Cell Res.*, **296**, 245–255.
37. Cossu, G. and Sampaolesi, M. (2007) New therapies for Duchenne muscular dystrophy: challenges, prospects and clinical trials. *Trends Mol. Med.*, **13**, 520–526.
38. O'Brien, K.F. and Kunkel, L.M. (2001) Dystrophin and muscular dystrophy: past, present, and future. *Mol. Genet. Metab.*, **74**, 75–88.
39. Sato, K., Yokota, T., Ichioka, S., Shibata, M. and Takeda, S. (2008) Vasodilation of intramuscular arterioles under shear stress in dystrophin-deficient skeletal muscle is impaired through decreased nNOS expression. *Acta Myol.*, **27**, 30–36.
40. Wehling, M., Spencer, M.J. and Tidball, J.G. (2001) A nitric oxide synthase transgene ameliorates muscular dystrophy in mdx mice. *J. Cell Biol.*, **155**, 123–131.
41. Wehling-Henricks, M., Lee, J.J. and Tidball, J.G. (2004) Prednisolone decreases cellular adhesion molecules required for inflammatory cell infiltration in dystrophin-deficient skeletal muscle. *Neuromuscul. Disord.*, **14**, 483–490.
42. Barleon, B., Sozzani, S., Zhou, D., Weich, H.A., Mantovani, A. and Marme, D. (1996) Migration of human monocytes in response to vascular endothelial growth factor (VEGF) is mediated via the VEGF receptor flt-1. *Blood*, **87**, 3336–3343.
43. Deasy, B.M., Feduska, J.M., Payne, T.R., Li, Y., Ambrosio, F. and Huard, J. (2009) Effect of VEGF on the regenerative capacity of muscle stem cells in dystrophic skeletal muscle. *Mol. Ther.*, **17**, 1788–1798.
44. Dawson, D., Vincent, M.A., Barrett, E.J., Kaul, S., Clark, A., Leong-Poi, H. and Lindner, J.R. (2002) Vascular recruitment in skeletal muscle during exercise and hyperinsulinemia assessed by contrast ultrasound. *Am. J. Physiol. Endocrinol. Metab.*, **282**, E714–E720.
45. Lindbom, L. (1983) Microvascular blood flow distribution in skeletal muscle. An intravital microscopic study in the rabbit. *Acta Physiol. Scand. Suppl.*, **525**, 1–40.
46. Crosbie, R.H. (2001) NO vascular control in Duchenne muscular dystrophy. *Nat. Med.*, **7**, 27–29.
47. Christov, C., Chretien, F., Abou-Khalil, R., Bassez, G., Vallet, G., Authier, F.J., Bassaglia, Y., Shinin, V., Tajbakhsh, S., Chazaud, B. *et al.* (2007) Muscle satellite cells and endothelial cells: close neighbors and privileged partners. *Mol. Biol. Cell*, **18**, 1397–1409.
48. Germani, A., Di Carlo, A., Mangoni, A., Straino, S., Giacinti, C., Turrini, P., Biglioli, P. and Capogrossi, M.C. (2003) Vascular endothelial growth factor modulates skeletal myoblast function. *Am. J. Pathol.*, **163**, 1417–1428.
49. Yan, H., Guo, Y., Zhang, P., Zu, L., Dong, X., Chen, L., Tian, J., Fan, X., Wang, N., Wu, X. *et al.* (2005) Superior neovascularization and muscle regeneration in ischemic skeletal muscles following VEGF gene transfer by rAAV1 pseudotyped vectors. *Biochem. Biophys. Res. Commun.*, **336**, 287–298.
50. Borselli, C., Storrie, H., Benesch-Lee, F., Shvartsman, D., Cezar, C., Lichtman, J.W., Vandenburgh, H.H. and Mooney, D.J. (2005) Functional muscle regeneration with combined delivery of angiogenesis and myogenesis factors. *Proc. Natl Acad. Sci. USA*, **107**, 3287–3292.
51. Asakura, A., Lyons, G.E. and Tapscott, S.J. (1995) The regulation of MyoD gene expression: conserved elements mediate expression in embryonic axial muscle. *Dev. Biol.*, **171**, 386–398.
52. Abramoff, M.D., Magelhaes, P.J. and Ram, S.J. (2004) Image processing with ImageJ. *Biophotonics Int.*, **11**, 36–42.
53. Baltgalvis, K.A., Call, J.A., Nikas, J.B. and Lowe, D.A. (2009) Effects of prednisolone on skeletal muscle contractility in mdx mice. *Muscle Nerve*, **40**, 443–454.
54. Sonnemann, K.J., Fitzsimons, D.P., Patel, J.R., Liu, Y., Schneider, M.F., Moss, R.L. and Ervasti, J.M. (2006) Cytoplasmic gamma-actin is not required for skeletal muscle development but its absence leads to a progressive myopathy. *Dev. Cell.*, **11**, 387–397.
55. Clark, A.D., Youd, J.M., Rattigan, S., Barrett, E.J. and Clark, M.G. (2001) Heterogeneity of laser Doppler flowmetry in perfused muscle indicative of nutritive and nonnutritive flow. *Am. J. Physiol. Heart Circ. Physiol.*, **280**, H1324–H1333.
56. Asakura, A., Komaki, M. and Rudnicki, M. (2001) Muscle satellite cells are multipotential stem cells that exhibit myogenic, osteogenic, and adipogenic differentiation. *Differentiation*, **68**, 245–253.
57. Asakura, A. and Rudnicki, M.A. (2002) Side population cells from diverse adult tissues are capable of *in vitro* hematopoietic differentiation. *Exp. Hematol.*, **30**, 1339–1345.
58. Asakura, A., Hirai, H., Kablar, B., Morita, S., Ishibashi, J., Piras, B.A., Christ, A.J., Verma, M., Vineretsky, K.A. and Rudnicki, M.A. (2007) Increased survival of muscle stem cells lacking the MyoD gene after transplantation into regenerating skeletal muscle. *Proc. Natl Acad. Sci. USA*, **104**, 16552–16557.
59. Sabourin, L.A., Girgis-Gabardo, A., Seale, P., Asakura, A. and Rudnicki, M.A. (1999) Reduced differentiation potential of primary MyoD$^{-/-}$ myogenic cells derived from adult skeletal muscle. *J. Cell Biol.*, **144**, 631–643.
60. Thompson, L.V., Durand, D., Fugere, N.A. and Ferrington, D.A. (2006) Myosin and actin expression and oxidation in aging muscle. *J. Appl. Physiol.*, **101**, 1581–1587.